CHAPTER 3.

Kinetics and Mechanism of the β- to α-$CuAlCl_4$ Phase Transition: A Time-Resolved ^{63}Cu MAS NMR and Powder X-Ray Diffraction Study

Haiming Liu[†], Roger M. Sullivan[‡], Jonathan C. Hanson[§], Clare P. Grey[†*], James D. Martin[‡*]

Department of Chemistry, North Carolina State University, Raleigh, NC 27695-8204; Department of Chemistry, State University of New York at Stony Brook, Stony Brook, NY 11794-3400; and Department of Chemistry, Brookhaven National Laboratory, Upton, NY 11973

*Corresponding authors

[†]State University of New York at Stony Brook

[‡]North Carolina State University

[§]Brookhaven National Laboratory

(As Published in *Journal of the American Chemical Society*; **2001**; *123*, 7564-7573.)

Abstract

The β- and α-phases of $CuAlCl_4$ have been characterized by solid state ^{27}Al and ^{63}Cu magic angle spinning nuclear magnetic resonance. The very short spin-lattice relaxation times of the copper spins, and the sensitivity of the I=3/2 ^{63}Cu nucleus to the small differences in the local structure of Cu in the two phases, allowed ^{63}Cu spectra to be acquired in very short time periods (1 minute), in which the β and α phases were clearly resolved. This time resolution was exploited to follow the phase transition from the pseudo-hexagonal close-packed β-$CuAlCl_4$ into the pseudo-cubic close-packed α-$CuAlCl_4$, which occurs above 100 ºC. *In situ* time-resolved ^{63}Cu MAS NMR and synchrotron x-ray diffraction experiments were used to measure the kinetics of this phase transition as a function of temperature. The transformation was shown to be a first-order phase transition involving no intermediate phases with an activation energy of 138 kJ/mol. The kinetic data obey a first order Avrami-Erofe'ev rate law. A one-dimensional growth mechanism is proposed that involves a combination of Cu^+ ion self-diffusion and a translational reorganization of the close-packed anion layers imposed by the periodic rotations of [$AlCl_4^-$] tetrahedra. This β to α phase transformation can be induced at ambient temperatures by low partial pressures of ethylene.

3.1. Introduction

Understanding the factors that control polymorphism is important for the rational design and synthesis of crystalline materials that exhibit targeted physical properties,[1] just as control of isomerism is critical in, for example, natural product synthesis. In biology, only L-amino acids are used in protein synthesis and the enzymes that catalyze the reactions, do not recognize the D-enantiomers. Similarly in solid state chemistry two polymorphs of a material frequently exhibit dramatically different properties. For example, the wide band-gap semiconductor SiC crystallizes in numerous polymorphs, the most common being the 3C-SiC polymorph with a cubic diamond-type lattice and 6H-SiC with a hexagonal lattice.[2] The 3C-polymorph is widely utilized as the abrasive, carborundum, and has a band gap of 2.39eV, whereas the 6H-SiC is the optimal phase for high-temperature and high power devices with a 2.86eV band gap suitable for blue light emitting diodes. In the absence of a mechanistic understanding, reaction design to achieve desired products is only an empirical endeavor. While a detailed understanding of organic reaction mechanisms is foundational to the modern pharmaceutical industry, a mechanistic understanding of solid-state chemistry is still in its infancy. Increasingly, measurements of the kinetics and thermodynamics of solid-state phase transitions in bulk solids[3] and nanoparticles[4] have been reported, but microscopic descriptions of the atomic motions involved, particularly for reconstructive phase transitions (i.e., where bonds are broken and formed) reaction are rarely articulated. In this paper, we present the kinetics of a phase change between two pseudo close-packed solids, and propose a plausible atomistic mechanism for the transition based on the dimensionality of the growth process,

combined with the known activation energies for the different motions that are involved in the transformation. Furthermore, breaking these solids into recognizable molecular-type sub-units permits an analysis of the vibrational modes present in the solid which provide insight into the molecular motions that may help to drive the phase transition.

From the earliest considerations of how hard spheres pack to form crystalline materials, close-packed models have provided a powerful way to visualize the structure of a variety of materials.[5] The simplest two forms of stacking close-packed layers, hexagonal close packing (*hcp*: ABAB...) and cubic close packing (*ccp*: ABCABC...), are found in pure elements, alloys and a variety of ionic and covalent compounds. Many carbides, nitrides, sulfides and halides exhibit a polymorphism that can be described in terms of these stacking sequences of close-packed atomic layers.[6] However, the mechanisms of the solid-solid phase transformations, which inter-convert these structure-types are less well defined. A shearing mechanism is the simplest means to reshuffle the close-packed layers from one stacking pattern to another. This is the mechanism proposed for phase transitions between *ccp* and *hcp* lattices in elemental solids such as Xe, Ca, Sc, Co and La.[7,8] A new level of complexity is introduced by considering a close-packed sublattice with additional atoms occupying interstitial sites. The wurtzite (*hcp*) and sphalerite (*ccp*) forms of ZnS are archetypal materials with a close-packed anion sublattice and cations in the tetrahedral interstices.[9] At 1024 °C, ZnS undergoes a reversible phase transition between the low-temperature sphalerite-phase and the high-temperature wurtzite-phase.[6] Both ZnS phases are observed at room temperature; the *hcp* wurtzite phase being metastable with respect to the *ccp* sphalerite phase. Cuprous halides also exhibit ZnS-like high temperature *hcp* and ambient temperature *ccp* phases.[10] Here

the bond breaking and making required for the reconstructive transition between the *hcp* and *ccp* polymorphs of such an AX material appears to be facilitated by lattice defects.[11] The ionic conductor AgI exhibits a metastable *ccp* phase, which coexists with the thermodynamically stable *hcp* phase at room temperature. Unlike the enantiotropic phase transition of ZnS, there is no characteristic transition temperature between the two phases for the monotropic phase-transition in AgI. This transformation is proposed to occur by the rearrangement of silver cations, which is then followed by a layer-by-layer reorganization of the iodides.[12] In an MX_2 cristobalite-type lattice, close packing of the anions can be observed when the ionic radius ratios allow M-X-M angles of 109.5º, as observed for α- and δ-$ZnCl_2$.[13, 14] While shearing vectors can be described to relate these *ccp* and *hcp* lattices, it seems unlikely that the atomic motions by which more complex materials actually transform are described by such a mechanism. Intermediate phases may occur on the pathway between *hcp* and *ccp* sublattices and a description of such a network transformation through the hypothetical "C9-MX_2" structure has been suggested.[15] Intermediate structures have been observed by variable temperature powder X-ray diffraction (PXRD) on transforming from the *hcp*-to *ccp*-type lattices of Cu_2Te.[16]

We have been investigating a series of $CuAlCl_4$ structures, with a view towards the construction of reactive open-framework materials.[17, 18] These materials may be considered as halide analogs of aluminophosphates. The apparent flexibility of the frameworks of these materials allows chemisorption of small gas molecules such as ethylene, forming a series of adduct phases.[19] The two polymorphs found so far, α- and β-$CuAlCl_4$, are differentiated by their *hcp* and *ccp* anionic sublattices, respectively, the β-phase being metastable with respect to the α-phase under ambient conditions. The low

temperature at which these two solids interconvert (~100 ºC) [20] as well as the spectroscopic handles of ^{27}Al and ^{63}Cu NMR makes this system ideally suited for an investigation of the mechanism of transformation between structures based on the archetypal *hcp* and *ccp* lattices. The β-$CuAlCl_4$ phase is prepared by rapid thermal quenching of the molten mixed metal halide and crystallizes in the orthorhombic space group $Pna2_1$. The α-phase forms on gradual cooling of a CuCl - $AlCl_3$ melt and crystallizes in the tetragonal space group $P\bar{4}2c$. Both phases contain alternating, corner sharing, $CuCl_{4/2}$ and $AlCl_{4/2}$ tetrahedra. Here we report an investigation of the mechanism of the conversion from the β to the α phase using a combination of time-resolved synchrotron X-ray powder diffraction (time-resolved PXRD) and magic angle spinning nuclear magnetic resonance (MAS NMR). The sensitivity of the quadrupolar ^{27}Al (I = 5/2, 100% natural abundance) and ^{63}Cu (I = 3/2, 69% natural abundance) nuclei to the local site symmetry are exploited to follow the phase transition. On the basis of kinetic data we propose a mechanism for the interconversion of these *hcp*- and *ccp*-derived structures. Utilizing both *in situ* time-resolved PXRD and *ex situ* ^{63}Cu MAS NMR we also demonstrate that exposure of β-$CuAlCl_4$ to low ethylene pressures induces a conversion from the β- to α-phase at room temperature, prior to adduct formation.

3.2. Experimental

Materials: β-$CuAlCl_4$ was prepared by quenching molten $CuAlCl_4$ (m.p. = 235 ºC), according to the literature preparation.[20] Two preparations were used for the kinetic

studies, one quenched from a 260 °C melt, denoted β-$CuAlCl_4^{(260°C)}$, and the other quenched from a 245 °C melt, denoted β-$CuAlCl_4^{(245°C)}$. Ethylene gas was used as purchased from Specialty Gas.

Powder X-ray Diffraction: Time-resolved PXRD experiments were performed at the X7B beamline of the National Synchrotron Light Source at Brookhaven National Laboratory, equipped with a translating image plate (TIP) system mounted on a four circle Huber diffractometer in a Debeye-Scherrer collection geometry.[21] Image plates (20x40 cm Fuji type IP) were scanned using a Fuji BAS2000 scanner.[22] The wavelength, sample-to-detector distance, tilting angle of the IP and zero shift position of the IP for the data collection were determined by using the 'fit2d' software package to analyze the full Debeye-Scherrer rings of the external standard LaB_6.[23] Wavelengths of 1.0014 and 0.9420 Å were determined for the variable temperature and ethylene sorption experiments, respectively. The time-resolved data collected on TIP system were processed, by using software written by Poul Norby for X7B.[21] Powdered β-$CuAlCl_4$ was placed in 0.7 mm fused silica capillaries and sealed with a torch, then aligned on a goniometer head so that it could be rotated in the synchrotron X-ray beam. A ceramic heater placed 3 mm from the sample was utilized to ramp the temperature at 4 °C/min from 30 °C to 190 °C, during which time diffraction data were collected. Ethylene sorption PXRD patterns were collected in a similar fashion utilizing an electronically controlled gas manifold to switch between vacuum and 100 Torr of ethylene.[24] Rietveld refinement of the structure was performed using GSAS.[25] The background was fit with a Fourier sum of cosine functions and the peak shape was fit by a pseudo-Voigt function.

NMR experiments: Variable temperature ^{27}Al and ^{63}Cu MAS NMR experiments were performed using a double-tuned Chemagnetics 5 mm probe in a CMX-360 spectrometer at operating frequencies of 93.8 and 95.5 MHz, respectively. The radiofrequency field strengths for ^{27}Al and ^{63}Cu were approximately 60 kHz. A single-pulse sequence with small flip angles (pulse width of 1 μs) was used to acquire all the MAS spectra. Spinning rates of 10.0 kHz and recycle delays of 1 s were used, unless specifically noted. Time-resolved ^{63}Cu MAS NMR measurements of the kinetics of the phase transition utilized a recycle delay of 0.1 s and 600 free induction delays were acquired per time interval. ^{27}Al and ^{63}Cu chemical shifts are referenced relative to a saturated aqueous $Al_2(SO_4)_3$ solution at 0 ppm and solid CuCl at –319 ppm,[26] respectively, as external standards. Temperature calibration was performed on a sample of solid $Pb(NO_3)_2$ spun at 10.0 kHz by monitoring the ^{207}Pb chemical shift as a function of temperature, as reported.[27]

NMR Studies of Ethylene Sorption: Room temperature ^{27}Al and ^{63}Cu MAS NMR spectra were obtained for the sample prior to and after exposure to 100 Torr of ethylene for 30 minutes, in order to examine the effect of low pressures of ethylene on the β to α phase transition. The sample of β-$CuAlCl_4$ was packed into a 3.4 mm Kel-F insert under an N_2 atmosphere, then exposed to ethylene using an apparatus modeled after the CAVERN design,[28] such that the sample was sealed under the ethylene atmosphere with an air-tight cap.

Simulations of NMR spectra: Numerical simulations of ^{27}Al and ^{63}Cu MAS NMR spectra were performed with programs developed in the GAMMA environment.[29] Two independent programs, both employing an efficient time propagation method based on

Floquet theory, were used to simulate the effect of the first- and second-order quadrupolar interactions on the experimental MAS NMR lineshapes of these quadrupolar nuclei.[30] Other spin interactions such as chemical shift anisotropy (CSA) and dipolar coupling were not taken into account when modeling the spectra, except for CSA in the simulation of the ^{63}Cu MAS NMR spectrum of α-$CuAlCl_4$.

3.3. Results

Powder X-Ray Diffraction: The time-resolved powder X-ray diffraction pattern of β-$CuAlCl_4$ during a temperature ramp is shown in Figure 1 (in the temperature range from 45 to 170 ºC). As the temperature increases, the pattern of the β-phase gradually disappears as the α-phase pattern appears. No intermediate phase is observed on going from the β- to α–phase, rather, both phases coexist in the same diffractogram, at approximately 120 ºC. Furthermore, there are no discernable changes in the line shape for any reflections as the phase transition progresses. The presence of reflections with similar d-spacings in both phases, corresponding to the distance between close-packed anion layers, (β-$CuAlCl_4$: 002 reflection at 18.82° 2θ (3.06 Å); α-$CuAlCl_4$: 112 reflection at 18.86° 2θ (3.06 Å)) is indicative of the common structural features. Rietveld refinements of the lattice parameters at room temperature and at approximately 120 °C were performed and the results are summarized in Table 1. A small decrease in volume per formula unit is observed between the β- and α- phases at all temperatures.

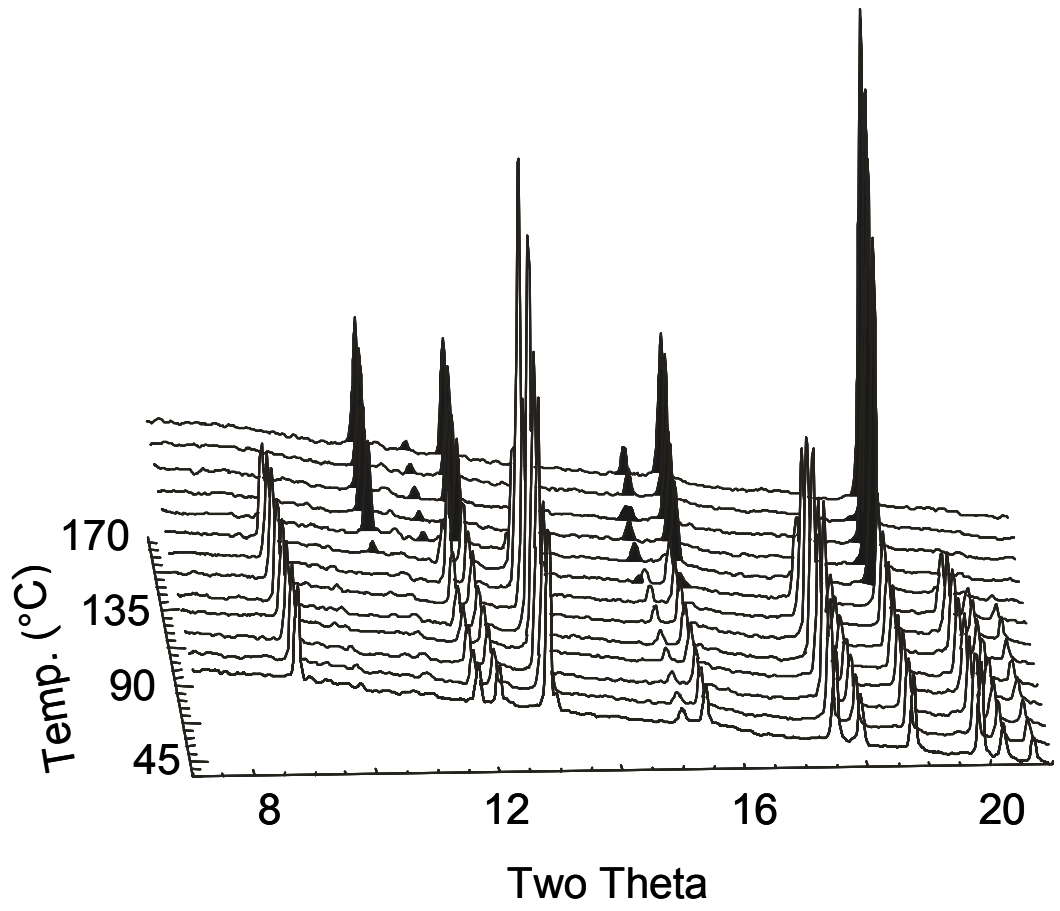

Figure 3.1. Variable temperature time resolved powder X-ray diffraction pattern showing the transformation from β-$CuAlCl_4$ to α-$CuAlCl_4$ (shaded black) upon heating at 4 °C/min.

Table 3.1. Cell parameters of β- and α-$CuAlCl_4$ at room temperature and at the phase transition temperature, obtained from PXRD.

Phase	T (°C)	a (Å)	b (Å)	c (Å)	Vol. ($Å^3$)	Z	Vol ($Å^3$) / Z
α-$CuAlCl_4$	20	5.438(1)	5.438(1)	10.096(1)	298.557(3)	2	149.279(3)
α-$CuAlCl_4$	120	5.488(1)	5.488(1)	10.094(1)	303.960(3)	2	151.980(3)
β-$CuAlCl_4$	20	12.8388(5)	7.6455(3)	6.1264(3)	601.362(1)	4	150.340(1)
β-$CuAlCl_4$	120	12.897(1)	7.720(1)	6.154(1)	612.652(3)	4	153.163(3)

^{27}Al MAS NMR: The room temperature ^{27}Al MAS NMR spectra of the β- and α-phases are shown in the bottom of Figures 2a and 2b, respectively. A single sharp isotropic resonance at 97 ppm, consistent with the presence of a single crystallographic aluminum site, is observed for both phases. This shift is typical for ^{27}Al tetrahedrally coordinated to four chloride anions.[31] No broadening of the centerband from the second-order quadrupolar interaction was observed, indicating that both sites have small quadrupolar coupling constants (QCC). Spinning sideband patterns due to the ^{27}Al satellite transitions are observed over a wide range of frequencies, but the sideband manifold of β-$CuAlCl_4$ is broader than that of α-$CuAlCl_4$ (Figures 2a and 2b). A QCC of 0.48 MHz and an asymmetry parameter, η, of 0.2 were obtained from the simulation of the β-$CuAlCl_4$ spectrum (top of Figure 2a and Table 2). Since the sideband manifold is narrower in α-$CuAlCl_4$, more accurate values of the QCC and η of 0.25 MHz and 0.3, respectively, were obtained by simulating the spectrum collected at a slower spinning speed of 4 kHz (inset of Figure 2b and Table 2). These values are consistent with the symmetry of the tetrahedral Al sites in the β- and α-phases: the aluminum in β-$CuAlCl_4$ is coordinated to four non-equivalent chlorides,[20] consistent with the larger QCC and $\eta \neq 0$, while the aluminum in α-$CuAlCl_4$ is bound to four equivalent chlorides, with a smaller range of Cl-Al-Cl bond angles, giving rise to a smaller QCC. Despite the different site symmetries, the chemical environments of the aluminum in β- and α-$CuAlCl_4$ are similar, giving rise to the same chemical shift of 97 ppm in the ^{27}Al MAS

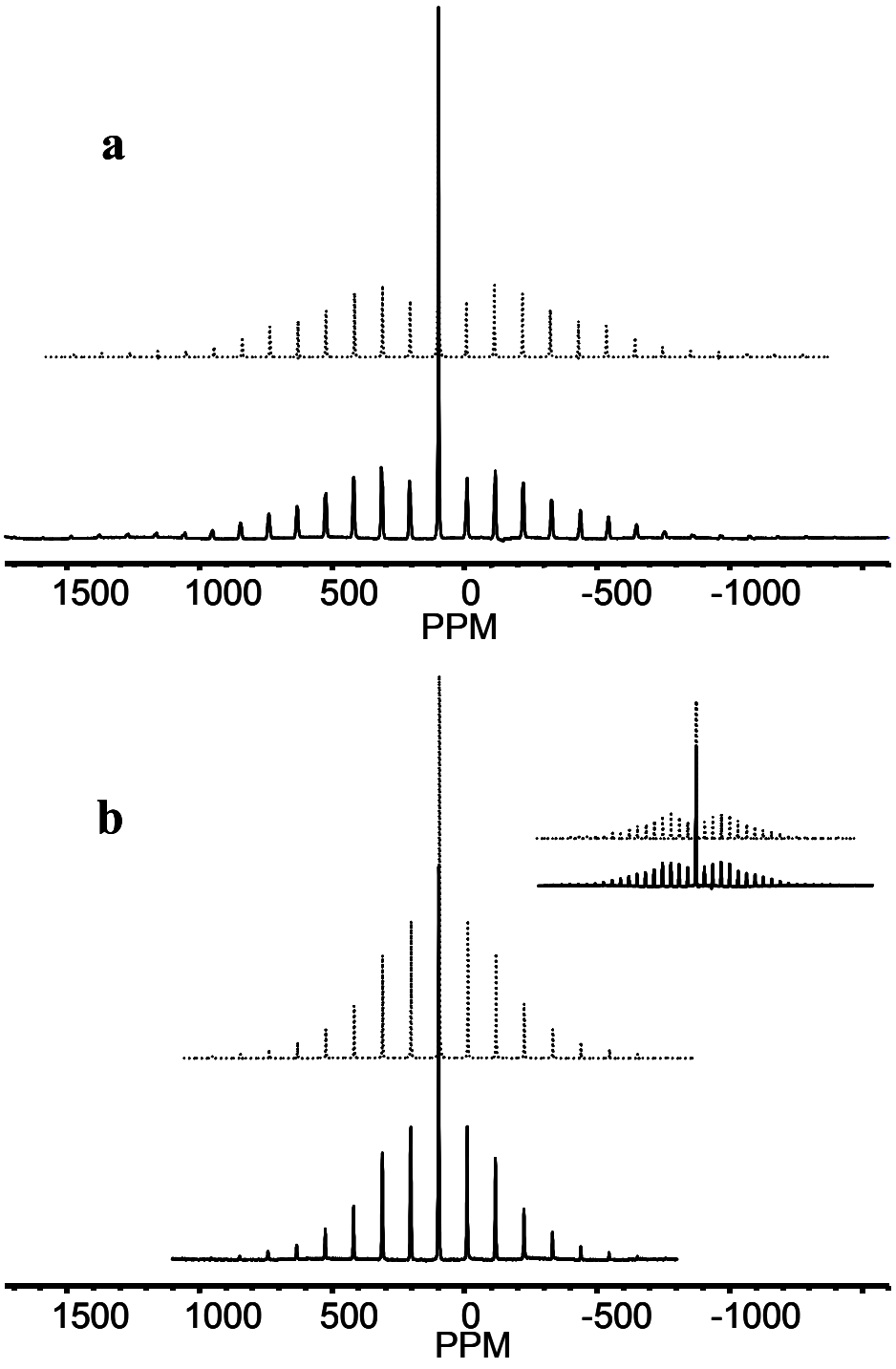

Figure 3.2. The experimental (bottom) and simulated (top) ^{27}Al MAS NMR spectra, at spinning speed of 10 kHz: a) β-$CuAlCl_4$, b) α-$CuAlCl_4$. The inset shows a spectrum of α-$CuAlCl_4$ collected at a spinning speed of 4 kHz (bottom) and the simulation (top).

NMR. Thus, when both phases are present, it will be difficult to determine the relative amount of each phase by using ^{27}Al MAS NMR.

^{63}Cu MAS NMR: The ^{63}Cu MAS NMR spectrum and simulation for β-$CuAlCl_4$ are shown in Figure 3a and b, respectively. A broad, second-order quadrupolar lineshape is observed corresponding to the single ^{63}Cu site. The small sharp peak at -431 ppm is due to the presence of a trace amount of α-$CuAlCl_4$. The spinning sidebands from the central transition of β-$CuAlCl_4$ (marked by asterisks) suggest that the second-order quadrupolar broadening of the central transition is larger than the spinning frequency. Values of δ_{iso} = -452 ppm, QCC = 4.3 MHz, and η = 0.8 were determined from the simulation.

The ^{63}Cu MAS NMR spectrum for α-$CuAlCl_4$ (Figure 3c) contains a sharp isotropic resonance at -431 ppm and large spinning sideband manifolds, due to the satellite transitions. Doublets are observed for the lowest-order spinning sidebands in Figure 3e, due to the significant difference between the second-order quadrupolar shift, $\delta^{(2)}$, of the central and satellite transitions.[32] The lower frequency set of sidebands is assigned to the central transition and displays an asymmetric shape, indicating a significant contribution to the broadening from the CSA. This broadening cannot be due to the dipole-dipole interactions in the rigid lattice, since these are reported to be only approximately 2 kHz for α-$CuAlCl_4$[33] and are, thus, negligible at a MAS spinning speed of 10 kHz. The CSA parameters, (span, Ω, = 105 ppm and skew, κ, = 1) were extracted from a static ^{63}Cu NMR spectrum of α-$CuAlCl_4$ (see Supporting Information).[34] The full α-$CuAlCl_4$ spectrum could be simulated with a δ_{iso} value of -429 ppm, a QCC of 0.9 MHz and η of

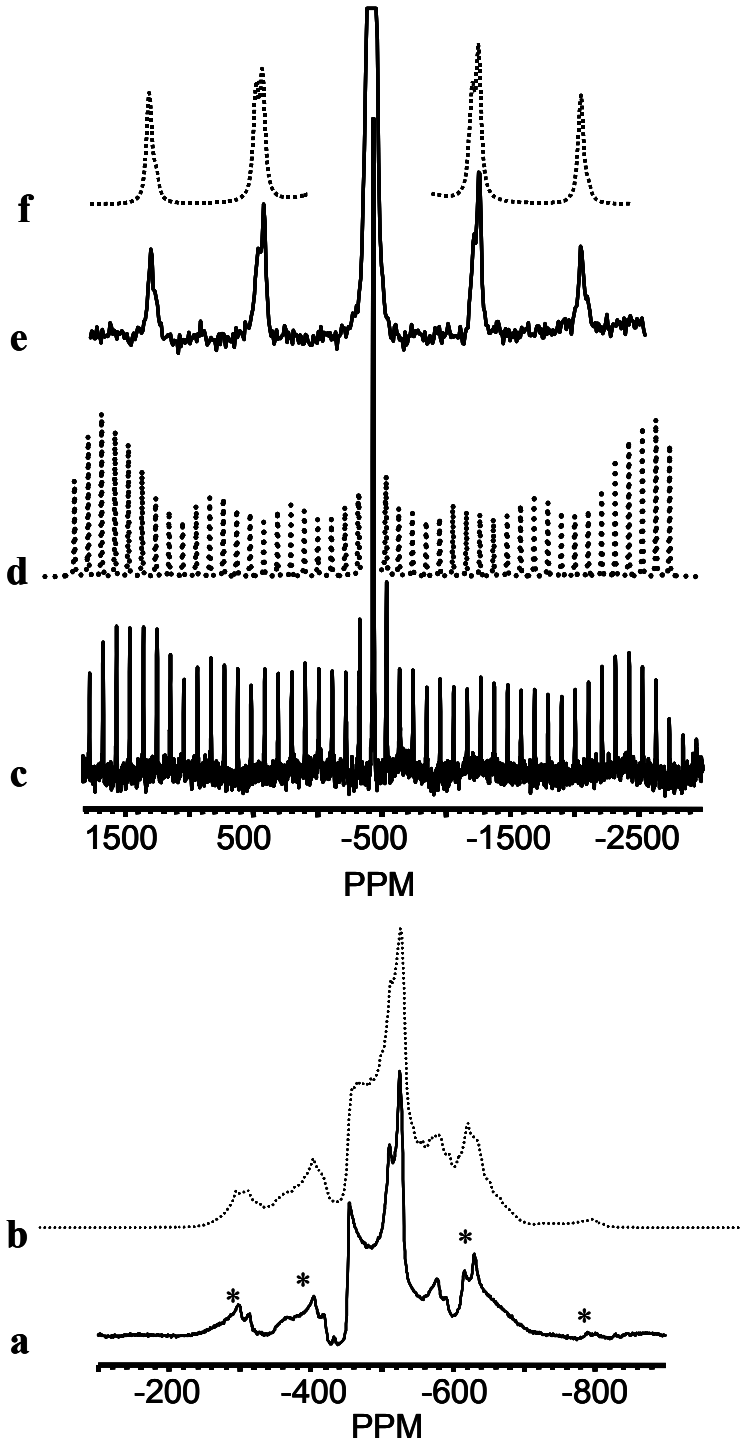

Figure 3.3. (a) The ^{63}Cu MAS NMR spectrum and (b) simulation for β-$CuAlCl_4$. Asterisks mark the spinning sidebands from the central transition. (c) The ^{63}Cu MAS NMR spectrum and (d) simulation for α-$CuAlCl_4$. An expanded view of the experimental (e) and simulated (f) spectra of α-$CuAlCl_4$ shows the splitting of the low order side bands.

Table 3.2. Quadrupolar interaction parameters obtained from simulations of ^{27}Al and ^{63}Cu MAS NMR spectra of β- and α-$CuAlCl_4$.

	^{27}Al			^{63}Cu		
	δ_{iso} (ppm)*	QCC (MHz)	η	δ_{iso} (ppm)	QCC (MHz)	η
β-$CuAlCl_4$	97	0.48	0.2	-452	4.3	0.8
α-$CuAlCl_4$	97	0.25	0.3	-429	0.9	0.05

* Isotropic ^{27}Al chemical shifts were directly taken from the spectra, and no correction due to the second-order quadrupolar shift, estimated to be less than 1 ppm, has been applied.

0.05, by including both the CSA and quadrupole interactions, and by assuming that the tensors that describe these two interactions are collinear (Figure 3f). This QCC is essentially identical to the value of 0.89 MHz previously measured by ^{63}Cu NQR.[33] Such a small QCC and the near-zero η are both consistent with the Cu site environment, in which Cu is coordinated to four equivalent chlorides with a $\bar{4}$ symmetry. The slight difference between the intensities of the observed and simulated higher-order sidebands is presumably due to the power-roll off effects observed under the experimental conditions. The ^{63}Cu NMR parameters for β- and α-$CuAlCl_4$ are summarized in Table 2.

Time-Resolved ^{63}Cu MAS NMR: The rapid spin-lattice relaxation, T_1, of the quadrupolar ^{63}Cu spins (~ 1 msec) allows for fast data acquisition with good signal-to-noise ratios. The course of a typical phase transition, measured at 135 ºC, is shown in Figure 4. Initially, the broad lineshape of β-$CuAlCl_4$ dominates the NMR spectrum. The sharp resonance due to the α-phase gradually grows in intensity, at the cost of the broad β-$CuAlCl_4$ resonance, and by 20 mins, dominates the spectrum. The extent of phase transition, α, is obtained by subtracting the integrated intensity of the α-$CuAlCl_4$ resonance at t_o = 0 sec from that at each time, *t*, and then normalizing it to the intensity upon completion of the phase transition. Kinetic data were collected at 105 °C, 125 °C, 135 °C, and 140 °C, and 100 °C, 110 °C, 120 °C, and 130 °C for the preparations of β-$CuAlCl_4$ quenched from melts at 260 °C and 245 °C, respectively. Plots of α versus *t* for β-$CuAlCl_4^{(260ºC)}$ at the four different temperatures are shown in Figure 5 (inset). The half-life for this phase transition varied from 11 min at 140 ºC, to 536 min at 100 ºC. To evaluate whether a common mechanism for this phase transformation is operative over

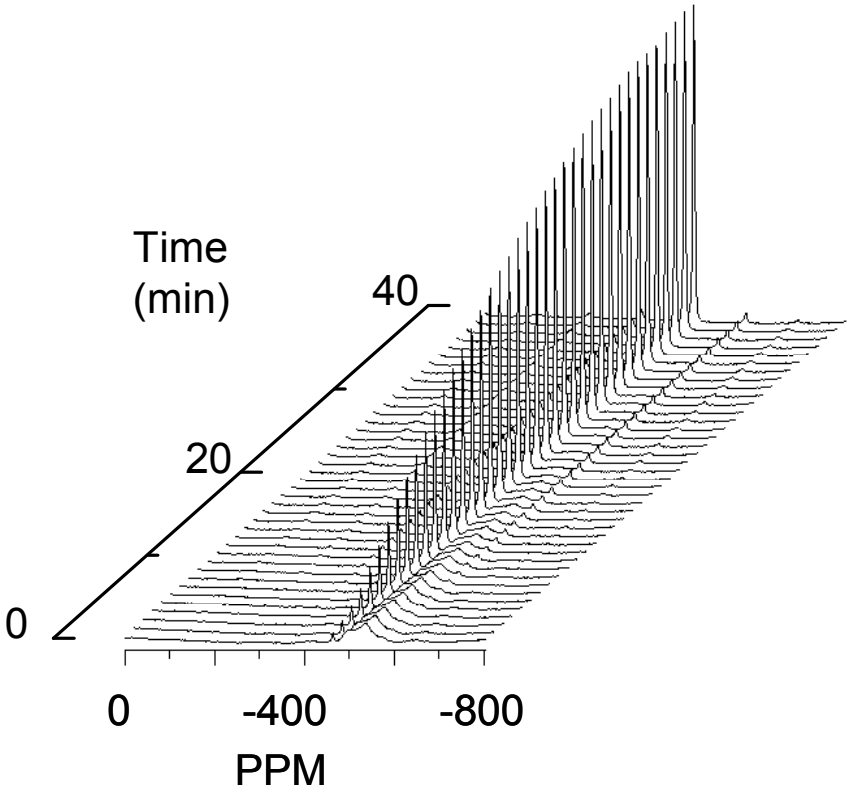

Figure 3.4. Time-resolved ^{63}Cu MAS NMR of the β- to α-$CuAlCl_4$ phase transition at 135 °C.

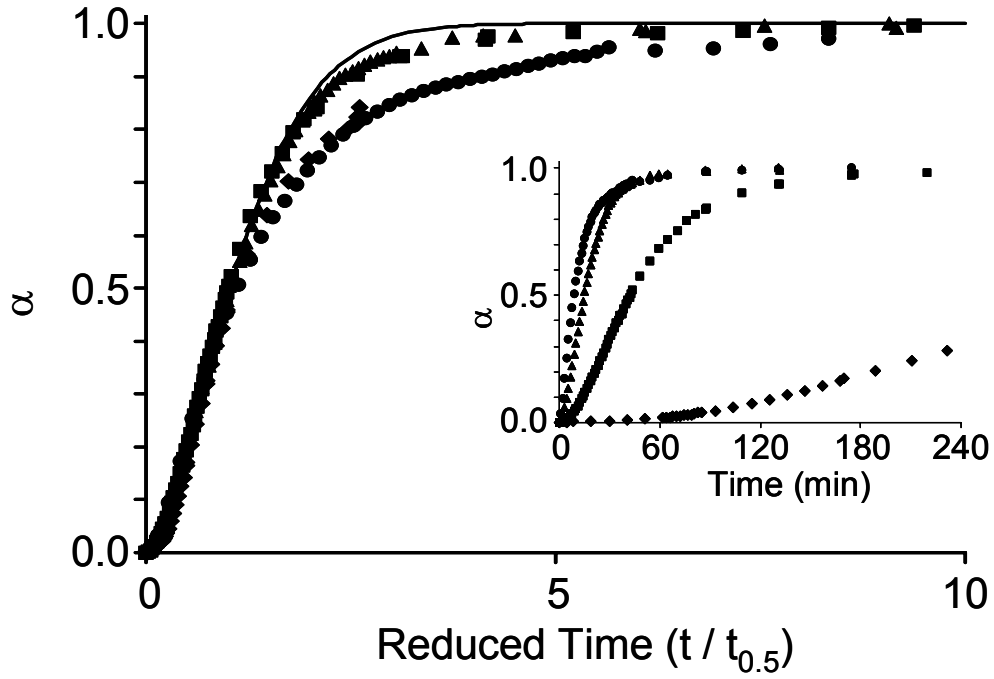

Figure 3.5. Reduced time plots of the fractional extent of transformation, α, as measured by ^{63}Cu MAS NMR: β-$CuAlCl_4^{(260°C)}$ at 105 °C (◆), 125 °C(■), 135 °C(▲), and 140 °C(●). The solid line is the calculated fits based on Avrami-Erofe'ev model with n = 1.5. The inset shows the fractional extent of transformation, α, as a function of real time.

the temperature range examined (i.e. isokinetic behavior) the extent of the phase transition, α, is also plotted as a function of the reduced time (Figure 5). The reduced time scale represents a normalization of all the time scales calculated by dividing the time at which the measurement is made, by the interpolated half-life (α = 0.5) for that particular isotherm.

Ethylene-induced β- to α-$CuAlCl_4$ phase transition: Both PXRD and NMR experiments were performed in order to investigate the phase transition that occurs in the presence of low pressures of ethylene. The pattern of β-$CuAlCl_4$ is observed in the time-resolved XRD at time zero (Figure 6). At t = 4 min, the sample was exposed to 100 Torr of ethylene and a rapid decrease in the intensity of the β-$CuAlCl_4$ reflections is seen. Two new sets of reflections grow in, which are assigned to α-$CuAlCl_4$ and the one equivalent adduct phase, $(C_2H_4)CuAlCl_4$.[19, 35]

A similar result is observed by ^{63}Cu MAS NMR spectroscopy. β-$CuAlCl_4$ shows a dramatic reduction of the broad β-$CuAlCl_4$ resonance after an *ex-situ* exposure to 100 Torr of ethylene, and the emergence of the sharp resonance of α-$CuAlCl_4$ (see Supporting Information). No additional ^{63}Cu MAS NMR resonances are observed. The phase transformation is confirmed by ^{27}Al MAS NMR: The ^{27}Al MAS NMR spinning sideband pattern of β-$CuAlCl_4$ is observed to change after exposure to ethylene, and becomes characteristic of α-$CuAlCl_4$ (see Supporting Information). No evidence for the characteristic broad ^{27}Al resonance of the one equivalent ethylene adduct is seen by ^{27}Al MAS NMR.[35]

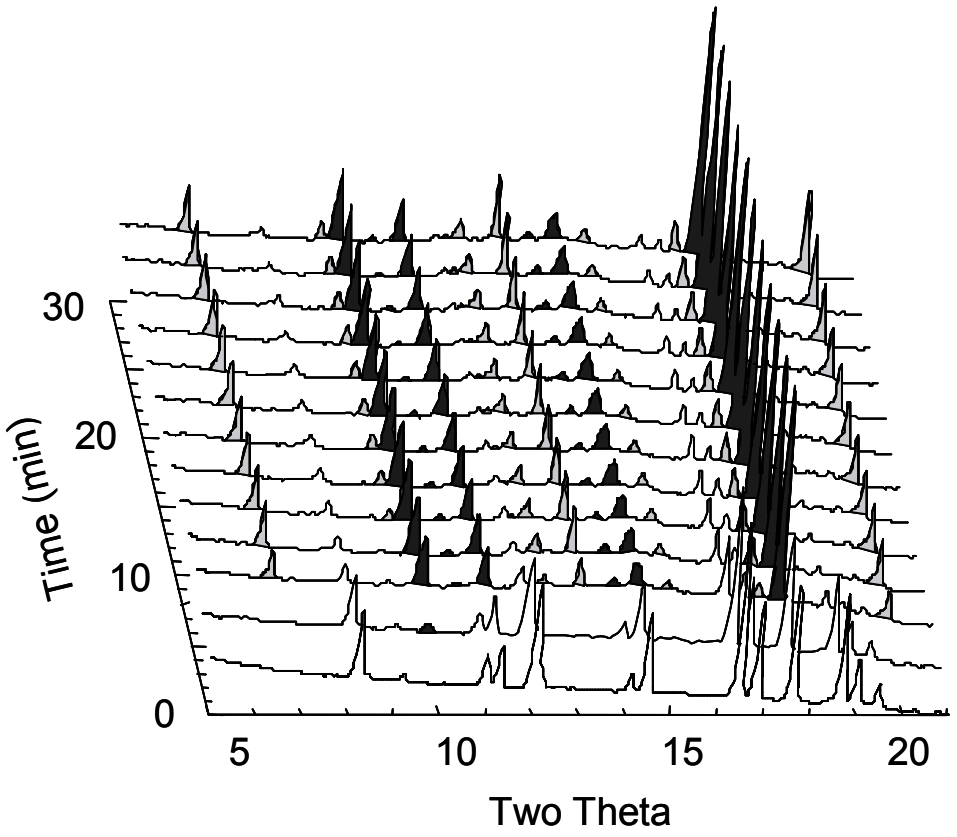

Figure 3.6. *In situ* time-resolved PXRD of the β- to α-$CuAlCl_4$ phase transition induced by 100 Torr of ethylene.

3.4. Discussion

^{63}Cu and ^{27}Al MAS NMR: The subtly different site symmetries and local distortions of Cu(I) in β- and α-$CuAlCl_4$ result in a significant difference in the ^{63}Cu QCC's (Table 2), and thus, dramatically different ^{63}Cu MAS NMR lineshapes. The ^{63}Cu QCC is zero for copper in an ideal tetrahedral ($\bar{4}3m$ site symmetry) geometry, whereas a range of QCC values of between 40 and 80 MHz has been reported for copper complexes with a variety of ligands.[36] The Cu cations are located on a general position in the β-phase in a slightly distorted tetrahedral environment, while in the α-phase, the copper cations are located on a special position with $\bar{4}$ symmetry. The QCCs of 4.3 and 0.9 MHz, respectively, are indicative of the very small deviations from ideal tetrahedral symmetry, and are consistent with the symmetry of the Cu local environments in their respective crystalline structures.[37]

The second-order quadrupolar interaction dominates the central transition resonance of the β-$CuAlCl_4$ ^{63}Cu MAS NMR, resulting in the significant linebroadening (Figure 3a). The second-order quadrupolar interaction also results in a shift in the center of gravity of the resonance to low frequency (the second-order quadrupolar shift,[32] $\delta_c^{(2)}$). A second-order quadrupolar shift can be so large that the apparent resonance may be well outside the chemical shift range expected for a given chemical environment. Thus, an isotropic chemical shift, δ_{iso}, was extracted from this spectrum in order to allow comparison with the different chemical environments of Cu(I). The δ_{iso} for ^{63}Cu in the β-

phase is -452 ppm, close to that of the α-phase, -429 ppm, as expected for their similar chemical environments (for CuCl, ^{63}Cu δ_{iso} = -319 [26]). This trend in the observed ^{63}Cu chemical shift δ(β-$CuAlCl_4$) < δ(α-$CuAlCl_4$) < δ(CuCl), correlates with the size of the average Cu-Cl-Cu angle, θ: (β-$CuAlCl_4$, $\theta = 111.75$ °) < (α-$CuAlCl_4$, $\theta = 110.95$ °) < (CuCl, $\theta = 109.47$ °).[20] A similar correlation between the ^{29}Si, ^{27}Al, or ^{71}Ga chemical shift and the average T-O-T' angle has been observed in zeolitic materials.[38] More data are clearly required to investigate the correlation for the ^{63}Cu shift in copper(I) metal halides, but we note that the shift of α-$CuGaCl_4$, with θ = 110.95 ° and δ_{iso} = -396 ppm,[20, 39] is consistent with this trend.

The line broadening due to the second-order quadrupolar interaction is negligible in the case of α-$CuAlCl_4$, resulting in a sharp isotropic resonance. The difference between the second-order quadrupolar shift for the satellite transitions and that of the central transition, $\Delta\delta$,[32] is however large enough to give rise to noticeable splitting in the low-order sidebands. The measured splitting, $\Delta\delta$ = 6 ppm (Figure 3e), corresponds to a QCC of 0.9 MHz assuming a value for η of 0, which is consistent with the value obtained from the simulation of the full spectrum, and with that measured previously by ^{63}Cu NQR.[33]

The ^{27}Al QCCs for the $[AlCl_4]^-$ tetrahedra in α- and β-$CuAlCl_4$ (0.25 and 0.48 MHz, respectively) are not as large as those of $[AlO_4]^{5-}$ tetrahedra in zeolites where typical ^{27}Al QCCs are 2-5 MHz.[40] Because the Al-Cl distance (2.1 Å) is longer than the Al-O distance (1.7 Å) and the charge on the chloride ions (-1) is lower than that on oxide ions (-2), a smaller electric field gradient (EFG) will be present (for similar environments)

accounting for the smaller QCC for an Al atom in a $[AlCl_4]^-$ tetrahedron, than in a similarly distorted $[AlO_4]^{5-}$ tetrahedron.

Time-Resolved PXRD: The time-resolved powder diffraction patterns shown in Figure 1 demonstrate that both phases coexist during the phase transformation and that no intermediate phases are formed. A small isothermal discontinuity in the molar volume is observed, which classifies the β- to α-phase transition as a first-order phase transition. First-order phase transitions are often characteristic of reconstructive phase transitions.

Kinetics: The progress of the β- to α-$CuAlCl_4$ phase transition at four isotherms, as followed by ^{63}Cu MAS NMR, is plotted as the fractional completion, α, vs. time in Figure 5 (inset). The plots for each of the four isotherms exhibit a sigmoidal shape, with time scales varying over three orders of magnitude. This sigmoidal shape is commonly observed for solid state reactions that are not diffusion-controlled,[41,42] and is typically analyzed by using the kinetic model proposed by Avrami[43] and Erofe'ev.[44] This model for phase transitions assumes that "germ nuclei" of the new phase are distributed randomly within the solid; following a nucleation event, grains grow throughout the old phase until the transformation is complete. The sigmoidal shape of these types of kinetic plots may then be analyzed by breaking the curve up into four regions: (i) an induction period ($0 < \alpha < 0.15$); (ii) an acceleratory region ($0.15 < \alpha < 0.5$); (iii) the deceleratory region ($0.5 < \alpha < 1$); and (iv) completion ($\alpha = 1$). The induction period tends to be dominated by nucleation events and the acceleratory tends to be dominated by growth. The deceleratory region results from the termination of growth upon impingement of different growth regions, or at grain boundaries.[41] It is in this region that considerable deviation between Avrami's single crystal model and data from powder samples is often

seen, typically due to variations in crystallite and/or grain size.[47] In contrast, deviation between the reduced time plots (and Sharp-Hancock plots as described below) for $0.15 \leq \alpha \leq 0.5$ is indicative of multiple reaction pathways as was observed, for example, in the intercalation of $CoCp_2$ by 2H-SnS_2.[41]

Avrami stated that a process is isokinetic when a constant ratio of the direction averaged rate of growth rate, *G*, and the probability of nucleation events per unit time, $\tilde{n}$, occurs (i.e. $G/\tilde{n}$ is constant for all isotherms).[43] The close overlay of the data in the acceleratory region for the four isotherms in Figure 5 is thus indicative of an isokinetic transformation for the β- to α-phase transition.

Sharp and Hancock utilized a plot of $\ln[-\ln(1-\alpha)]$ vs. $\ln(t)$, in order to explore the order of solid state reaction rate laws. The Sharp-Hancock plot, when linear over the acceleratory interval $0.15 \leq \alpha \leq 0.5$, is diagnostic of certain groupings of rate laws according to the slope, *n*, of eq 1:[45]

$$\ln[-\ln(1-\alpha)] = n \ln(t) + b \qquad (1)$$

An average slope of $n = 1.5(\pm 0.2)$, was obtained from the Sharp-Hancock plots of the four β-$CuAlCl_4^{(260ºC)}$ (Figure 7a) and four β-$CuAlCl_4^{(245ºC)}$ isotherms. This, as well as the sigmoidal shape of the α vs. *t* plot, suggest that the Avrami-Erofe'ev rate law given in eq 2 is operative for the β- to α-$CuAlCl_4$ phase transition.

$$[-\ln(1-\alpha)]^{1/n} = kt \qquad (2)$$

The term n in the exponent of eq 2 is equivalent to the slope obtained from the Sharp-Hancock plot. For phase boundary controlled reactions, such as described by eq 2, $n = \lambda + \beta$ where λ is the dimensionality of growth (1, 2, or 3) and β represents the contribution of the nucleation process and varies between 0 and 1 ($\beta = 0$ for instantaneous nucleation and $\beta = 1$ for a very slow nucleation rate).[43b] Thus, values of $n = 1 - 2$ are observed for one-dimensional growth, $n = 2 - 3$ for two-dimensional growth and $n = 3 - 4$ for three-dimensional growth.[41] The experimental data can be fit to the Avrami-Erofe'ev equation throughout the acceleratory region (Figure 5), by using a value for n of 1.5, indicating that this phase transition proceeds via a one-dimensional growth process. Furthermore, because the composition does not change throughout the phase transition the growth must be phase boundary controlled rather than diffusion controlled.[41] The data begin to deviate from the Avrami-Erofe'ev model in the decelatory region with the greatest deviation being observed for the highest and lowest temperature isotherms. The deviations from the model in the declaratory region are most pronounced in the $\beta^{(245°C)}$ sample; the differences most likely arising from variations in grain size as a result of sample preparation.

Rate constants, k, for each isotherm were determined by linear regression of the Sharp-Hancock plots, where the intercept, b, equals $n\ln(k)$ in the case of the Avrami-Erofe'ev equation (see Table I of Supporting Information for rate constants). The rate constants for each set of isotherms exhibit Arrhenius-type behavior as shown in Figure

7b. The activation energy, E_a, and prefactor, ν, as described in the Arrhenius equation, eq 3, were determined by the weighted linear regression of $\ln(k)$ vs. $1/T$.[46]

$$\ln(k) = \ln(\nu) + (E_a / RT) \qquad (3)$$

For β-$CuAlCl_4^{(260°C)}$, E_a = 139(6) kJ/mol, ν = 6×10^{14} s^{-1} ($\ln(\nu)$ = 34(2)), and for β-$CuAlCl_4^{(245°C)}$, E_a = 138(19) kJ/mol, $\nu = 6\times10^{14}$ s^{-1} ($\ln(\nu)$ = 34(6)). A slight difference is observed in the Arrhenius plots for the two sets of experiments utilizing β-$CuAlCl_4^{(260°C)}$ and β-$CuAlCl_4^{(245°C)}$ (Figure 7b), however, the difference lies well within the 95% confidence interval. Thus the quenching temperature has not significantly altered the number of germ nuclei and consequently, the observed rate.

Mechanistic Considerations: The process described by the rate equation is complex and involves both nucleation and growth. The Avrami-Erofe'ev model approximates the case where $G << \tilde{n}$.[47] Because the majority of growing nuclei will have formed during the induction period, $\alpha < 0.15$, the number of growing nuclei will be nearly constant throughout the acceleratory region of $0.15 \leq \alpha \leq 0.50$. Because this region is growth-dominated, the measured rate constants, and hence the Arrhenius parameters, describe the growth of the α-$CuAlCl_4$ phase; thus any proposed mechanism must be consistent with these.

In order to understand solid state phase transitions it is useful to consider the symmetry relationships between the space groups of the transforming phases.[48, 49] There are, however, no symmetry subgroup, supergroup relationships between the unit cells of

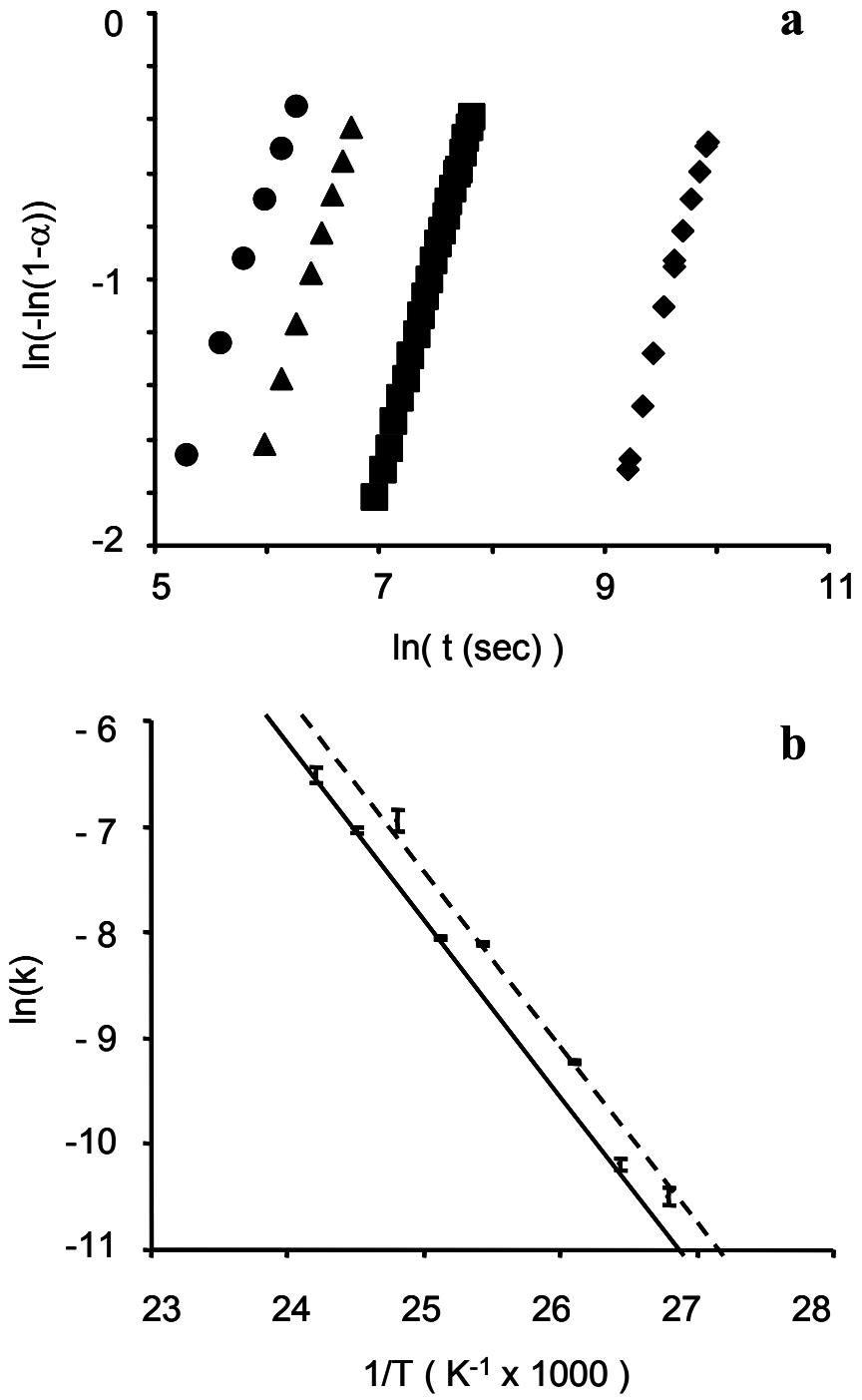

Figure 3.7. (a) Sharp-Hancock plots of the phase transition for β-$CuAlCl_4^{(260°C)}$ at 105 °C (◆), 125 °C(■), 135 °C(▲), and 140 °C(●). (b) Arrhenius plots of rate constants for β-$CuAlCl_4^{(245°C)}$ (solid line) and β-$CuAlCl_4^{(260°C)}$ (dashed line).

β- and α-$CuAlCl_4$. Nonetheless, β- and α-$CuAlCl_4$ share a common 4 × 4 anion layer in which aluminum and copper cations are distributed in 2 × 2 zigzag chains with strict Al/Cu alternation.[20] Six of these layers stack, in either a *hcp* or *ccp* sequence, to form a non-primitive hexagonal cell (a = b = 15.09Å, c = 18.48Å), which is the smallest cell common to both structure-types. Figure 8a illustrates a non-standard, distorted-hexagonal cell from the single crystal structure of β-$CuAlCl_4$ (a = 15.02 Å, b = 15.43 Å, c = 18.44 Å, α = 90.00 °, β = 90.00 °, γ = 120.90 °, Z = 24); and Figure 8b illustrates a non-standard, distorted-hexagonal cell from the single crystal structure of α-$CuAlCl_4$ (a = 14.91, b = 15.53, c = 18.52 Å, α = 90.00°, β = 86.12°, γ = 121.37°, Z = 24).

Phenomenologicaly, the structures of β- and α-$CuAlCl_4$ can be related by a shearing dislocation between the close-packed layers, which re-orders the stacking sequence (…ABABAB… to …ABCABC…). In a shearing mechanism the activation energy should be related to the enthalpy of the bond breaking at the phase boundary.[41,50] However, the dissociation energies of the Al-Cl (495 kJ/mol)[51] and Cu-Cl (383 kJ/mol)[52] bonds are significantly higher than the activation energy of the β- to α-$CuAlCl_4$ phase transition (138 kJ/mol), and furthermore are notably different from each other. Thus a shearing mechanism involving simultaneous bond breaking of Al-Cl and Cu-Cl bonds seems unlikely. Although a shearing mechanism is energetically disfavored, the energy cost in strain along a close-packed layer boundary is expected to be small because the molar volume change between the α- and β-phases is small. Furthermore, the negligible structural mismatch between the *hcp* and *ccp* layers minimizes the interfacial energy cost at the phase boundary.[53] The low energetic cost of this phase boundary in addition to the

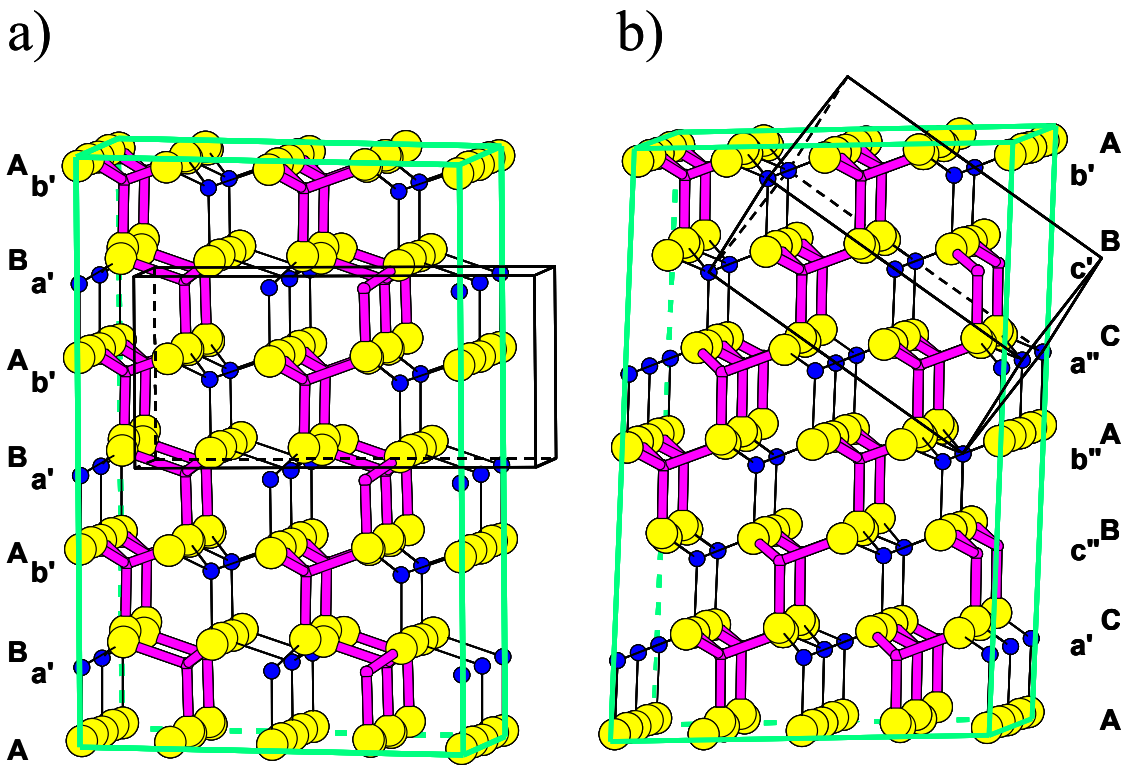

Figure 3.8. The stacking patterns of the distorted close-packed anion sublattice (capital letters) and the interstitial cations (lower case letters) which relate the two polymorphs of $CuAlCl_4$: a) non-standard, pseudo-hexagonal cell of β-$CuAlCl_4$, with one orthorhombic unit-cell outlined, b) non-standard, pseudo-hexagonal cell of α-$CuAlCl_4$ with one tetragonal unit-cell outlined.

one-dimensional-growth rate law suggests that a likely direction for growth of α-$CuAlCl_4$ is the unique crystallographic direction perpendicular to the close-packed (002) layers of β-$CuAlCl_4$. Thus mechanisms other than shear that can transpire at this close-packed phase boundary must be considered.

Literature values of Arrhenius parameters for processes such as copper self diffusion and tetrachloroaluminate reorientation in related systems are of interest since they indicate what kinds of atomic reorganization may occur at the phase boundary, and whether they are energetically feasible. For example, self-diffusion of Cu(I) in α-$CuAlCl_4$ (onset ~ 110 °C) is reported to have an E_a of 48.5 - 51.8 kJ/mol.[33] Cu(I) diffusion in the isostructural $CuAlBr_4$ is similar: E_a = 33.7 - 49.1 kJ/mol. The activation energies for $[AlCl_4]^-$ reorientation in $AgAlCl_4$ include a reorientation about a three-fold axis (onset ~ 120 °C), E_a = 82.2 kJ/mol and an isotropic reorientation (onset ~ 140 °C), E_a = 94.1 kJ/mol.[33] For $LiAlCl_4$, reorientation about either a two fold or three fold axis is reported to have an E_a of 95.6 kJ/mol.[54] Despite the range in measured activation energies for Cu^+ self-diffusion and $AlCl_4^-$ reorientation, the values are all sufficiently below that of the β- to α-$CuAlCl_4$ phase transformation such that these processes are energetically accessible for consideration with regard to the growth mechanism.

Mechanism for the β- to α-$CuAlCl_4$ Phase Transformation: A combination of $[AlCl_4]^-$ reorientations and Cu^+ self-diffusion can map each atom in the β-$CuAlCl_4$ structure (Figure 8a) onto a corresponding atom position in the α-$CuAlCl_4$ structure (Figure 8b). Because the copper cations are free to hop between tetrahedral interstices, we primarily consider the atomic motions required to reorganize the tetrachloroaluminate

sublattice, which may be described in terms of symmetry-allowed normal lattice and librational modes of the initial and final structures. The symmetry breaking event leading to the β- to α-phase transition occurs when the restoring forces relax the vibrationally excited state in the phase boundary to the new α-positions instead of restoring the atoms to the old equilibrium positions of the β-phase. In spite of the facility of copper ion self-diffusion, we will favor mechanistic descriptions that require a minimum of copper migration.

A schematic representation of the mechanism for the β- to α-$CuAlCl_4$ phase transition can be described by considering pairs of close-packed layers, Figure 9 and Table 3.3. As a point of reference, the yellow shaded chloride ions of the B-anion layer in Figure 9a are equivalent to atoms of the 'post-transformation' C-anion layer of Figures 9b, c and d; and the $[AlCl_4]^-$ tetrahedra will be classified with respect to the layer in which the apical chloride resides. The librations about the pseudo three-fold axis of each $[AlCl_4]^-$ tetrahedra (described by the dashed circles) are geometrically consistent with the close-packed layer description of the phase boundary. Rotation of the A-$[AlCl_4]^-$ tetrahedra by 60° (clockwise and counter clockwise, respectively, as represented by the black arrows in Figure 9a, about the Al-Cl bonds perpendicular to the close-packed layers will move the B-chlorides into the C positions of the α-phase. Coincident with the rotation of the A-$[AlCl_4]^-$ tetrahedra, the tetrachloraluminates with apical chlorides in the B-layer must translate to C-positions as shown by the gray arrows. Neither aluminum nor copper cations need move within this pair of close-packed layers, although the copper cations trade one set of chloride partners, to achieve the atomic arrangement of the α-

phase, Figure 9b. This translation shifts the non-transformed β-phase, such that it is now described with a …CBCB… repeat, with respect to the A-layer fixed as the origin of the transformation. No further rotation of the $[AlCl_4]^-$ tetrahedra is required to propagate the phase boundary through the CB pair of layers, Figure 9c → 9d, however, self-diffusion of the copper cations within this pair of layers is required. Translation of the copper cations by the same vector as the four host chlorides of its original tetrahedral interstice (the horizontal white arrows) would result in 1/4 of the C-chlorides (yellow) being coordinated to three metals (2 Cu and 1 Al) and 1/4 being coordinated only to one aluminum cation. This can be visualized by considering the cations above and below the C-layer chlorides if Figures 9b and 9c are superimposed (the yellow C-chlorides of the two figures are the same set of atoms). This violates the strict Cu-Cl-Al alternation observed in both the β- and α-phases. Migration of the copper cations within this new β-(CB) layers to neighboring tetrahedral interstices, as shown by the vertical hollow arrows in Figure 9c, reestablishes the Cu-Cl-Al alternation and results in the cation distribution observed for the α-(CB) layer. When viewed as the vector sum of these two translations, the copper atom migration is in a direction consistent the rotation of the A-layer $[AlCl_4]^-$. It is further interesting to note that this process maintains the network of 2 × 2 zigzag chains of $AlCl_{4/2}$ and $CuCl_{4/2}$ tetrahedra throughout the phase transition. (Alternate permutations of the directions of the tetrachloroaluminate rotation described in Figure 9 can also lead to the equivalent structural transformation.) As described in Table 3.3, this pair-wise 60º/0º rotation of tetrachloroaluminate anions in alternating close-packed layers exhibits a six-layer periodicity. Thus, it is tempting to speculate that the phase boundary may have a width of six close-packed layers. The translational component of the $[AlCl_4]^-$

Table 3.3. The six-layer periodicity for the movement of all β-$CuAlCl_4$ layers (colorless boxes) into the α-$CuAlCl_4$ stacking pattern (shaded boxes) is tabulated in a stepwise fashion. The tabulation lists the change in stacking patterns caused by three steps, in which a pair-wise 60º/0º rotation of tetrachloroaluminate anions in alternating close-packed layers is coupled with the translations necessary to maintain a close-packed anion sublattice.

A		B		C		A
b'		c"		a"	0º	b'
B		C		A		B
a'		b"		c'	60º	c'
A		B		C		C
b'		c"	0º	a"		a"
B		C		A		A
a'		b"	60º	b"		b"
A		B		B		B
b'	0º	c"		c"		c"
B		C		C		C
a'	60º	a'		a'		a'
A		A		A		A
β	→					α

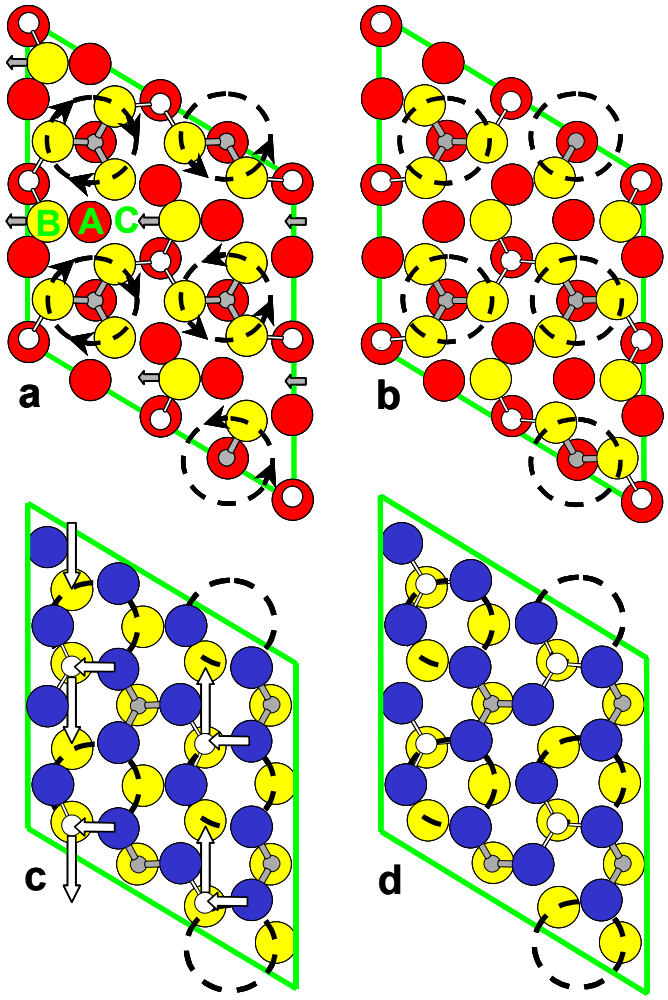

Figure 3.9. A schematic representation of the mechanism for the β- to α-$CuAlCl_4$ phase transition. Chlorides are colored red, yellow and blue, to identify them with 1st, 2nd and 3rd close-packed layers of Figure 3.8, respectively; copper cations are small white spheres; and aluminum cations are shaded gray. The labels A, B, and C indicate the locations of the chlorine atoms in the respective close-packed layers. Dashed circles indicate the arc of the tetrachloroaluminate libration, and arrows indicate a set of atomic motions that account for the phase transition. The β-AB layer (i.e., the 1st and 2nd layers) is shown in (a). The A-$[AlCl_4]^-$ tetrahedra, which contain one chlorine atom in the A-layer and three in the B-layer, undergo a 60º rotation while the apical chlorides of the B-$[AlCl_4]^-$ tetrahedra undergo a translation, yielding the α-AC layer as shown in (b). The movement of the B-$[AlCl_4]^-$ tetrahedra results in a shift of the lattice above the B layer, resulting in a change from BA to CB packing in the 2nd and 3rd layers (also described in Table 3.3). As shown in (c), the copper ions in-between the 2nd and 3rd layers have translated with their nearest neighbor chlorides (directed by the reorientation of the B-$[AlCl_4]^-$ tetrahedra), indicated by the white horizontal arrows. Self-diffusion of the copper cations to neighboring interstices (white vertical arrows) yields the α-CB layer, as shown in (d).

tetrahedra, on going from the β- to α-phase, accounts for the increase in the activation energies of the phase transformation compared to the component processes of Cu^+ self-diffusion and $AlCl_4^-$ reorientations.

While it is facile to visualize, the idea of tetrahedra rotating by 60° in one layer and 0° in the alternating layer is not very satisfactory from a mechanistic point of view. No single lattice librational mode (i.e. the symmetric or antisymmetric combinations of the rotational directions of the four $[AlCl_4]^-$ within C_{2v} point symmetry of the β-$CuAlCl_4$ unit cell) corresponds to this motion. However, a combination mode of the a_2 and b_1 30º librations (or the a_1 and b_2) within the two pairs of close-packed layers of β-$CuAlCl_4$ is a possible way to account for the overall 60º/0º atomic motions. In addition to $[AlCl_4]^-$ reorientation by means of the external librational modes, coupling with internal stretching and bending modes of the $[AlCl_4]^-$ tetrahedra must also be invoked because of the change in site symmetry.[55] An increased degeneracy of these internal modes will occur as the corner sharing aluminum- and copper-chloride tetrahedra adopt their higher site symmetries in α-$CuAlCl_4$. The space-group symmetry of β-$CuAlCl_4$ dictates a unique crystallographic direction (001), which orients the pseudo-three fold rotation axes of the tetrahedra with respect to the phase boundary. Such unique orientation is lost in α-$CuAlCl_4$, with four equivalent close-packed directions (112, 11-2, -1-12, -1-1-2). The degeneracy of the $[AlCl_4]^-$ librational modes in α-$CuAlCl_4$ makes it unlikely that any phase boundary will propagate in one unique direction as required for the β-phase. This degeneracy of lattice modes suggests the irreversibility of the phase transition is related to a large entropic barrier. In some respects, the space-group allowed librational

symmetry, which apparently directs this first-order phase transition, is reminiscent of symmetry driven second-order phase transitions,[48] and the more commonly understood symmetry controlled mechanisms of molecular reactions.[56]

Ethylene induced β- to α-$CuAlCl_4$ phase transition: We have previously reported the reversible sorption of ethylene by α-$CuAlCl_4$[19] However, exposure of β-$CuAlCl_4$ to low pressures of ethylene (<100 Torr) induces the β- to α-$CuAlCl_4$ phase transition to occur rapidly at room temperature, as observed by time-resolved PXRD (Figure 6) prior to adduct formation. The relative amount of the α-$CuAlCl_4$ with respect to the $(C_2H_4)CuAlCl_4$ adduct was observed to increase deeper into the sample capillary. (In the experimental setup a diffusion gradient through the capillary is normally observed.) The $(C_2H_4)CuAlCl_4$ phase is normally observed when α-$CuAlCl_4$ is exposed to less than 760 Torr of ethylene as well as upon desorption of ethylene from $(C_2H_4)_2CuAlCl_4$.[35] The transformation of β- to α-$CuAlCl_4$ upon exposure to 100 Torr of ethylene was also observed by ^{63}Cu and ^{27}Al MAS NMR (see Supporting information).

It is reasonable to propose that the sorption of very small amounts of ethylene create a population of extrinsic defects by cleavage of Cu-Cl bonds as is known to occur upon formation of the one equivalent adduct.[19c] Extrinsic defects will influence both nucleation and growth of the *ccp* phase. Such a model is reminiscent of the phase transformation between *hcp* and *ccp* ZnS in the presence of defects created by Cu^+ and Cl^- dopants,[11] and, the transformation from the metastable *ccp* phase of AgI to the stable *hcp* phase upon exposure to I_2 vapor.[57] Such extrinsic defects, and the accompanying

vacancies, facilitate the rearrangement of atoms needed to reorder the stacking sequence of the close-packed layers.[11]

3.5. Conclusions

Using *in situ* time-resolved ^{63}Cu MAS NMR and synchrotron PXRD, kinetic and activation parameters for the phase transformation from β- to α-$CuAlCl_4$ have been determined which provide the basis for an atomistic description of reaction mechanism. The MAS NMR parameters were successfully simulated and demonstrate the sensitivity of the ^{63}Cu nucleus to subtle changes in its environment. Time-resolved ^{63}Cu MAS NMR kinetic data for the phase transformation have been shown to obey a first-order Avrami-Erofe'ev rate law. The results of variable temperature time-resolved powder X-ray diffraction experiments show that the transformation of pseudo-hexagonal close-packed β-$CuAlCl_4$ into pseudo-cubic close-packed α-$CuAlCl_4$ is a first-order phase transition with no intermediate phase. These data suggest a one-dimensional growth mechanism, which involves a combination of Cu^+ self-diffusion and a translational reorganization of the close-packed anion layers imposed by the periodic rotations of $[AlCl_4]^-$ tetrahedra. This atomic re-ordering appears to be directed by the rotational and translational degrees of freedom allowed by the symmetry constraints of the crystalline lattice. A shearing mechanism and a mechanism involving random motion and reordering seem to be unlikely. This β- to α-$CuAlCl_4$ phase transition can also be induced by ethylene at ambient temperature, which may be due to creation of extrinsic defects.

This mechanistic study highlights the importance of considering the lattice symmetry in the understanding of first-order phase transitions and shows how simple arguments based on the energetics of individual molecular-type sub-units are useful for evaluating different transformation mechanisms. Molecular dynamics simulations may provide an ideal method to test our proposed model for the phase transition and the relative importance of the different vibrational modes. To trace possible pathways for first-order phase transitions it may be useful to consider the combination modes of allowed lattice librations, just as supergroup/subgroup relationships are used to describe and determine the allowed second-order phase transitions. Furthermore, the symmetry breaking events of the lattice reconstruction become possible only when the amplitude of the symmetry-allowed librations exceeds some threshold determined by the phase boundary. Finally, this mechanistic understanding suggests that degeneracy of the symmetry-allowed lattice librations may impact whether or not a given metastable phase can be isolated. More mechanistic examples are clearly required to explore the generality of some of these ideas, however, this latter suggestion in particular may represent a step towards the goal of rationally designing metastable materials.

Acknowledgements

Dr. Kwang Hun Lim is acknowledged for coding and help with the NMR simulations in the GAMMA environment. Michael Ciraolo is thanked for his help with the diffraction

experiments. Support of this work, via the contracts NSF DMR-9501370 and DMR-0072828, and DOE BES DE-FG02-96ER14681 and DE-AC02-98CH10886, is gratefully acknowledged. JDM and CPG are Cottrell Scholars of the Research Corporation.

Supporting Information Available: Static ^{63}Cu NMR spectrum and the simulation of α-$CuAlCl_4$; Table of rate constants; Calculation of the second-order quadrupolar shift, $\delta^{(2)}$, for an I=3/2 nuclear spin; The ^{63}Cu and ^{27}Al MAS NMR spectra of β-$CuAlCl_4$ before and after exposure to 100 Torr ethylene. This material is available free of charge via the Internet at http://pubs.acs.org.

3.6. References

1 a) Rao, C. N. R.; Gopalakrishnan, J. *New Directions in Solid State Chemistry*; Cambridge University Press: Cambridge, U.K., 1997; pp. 168-228. b) West, A. R. *Solid State Chemistry and It's Applications*; John Wiley and Sons: New York, 1989; p. 109 c) Seddon, K. R. Crystal Engineering. In *Crystal Engineering: The Design and Application of Functional Solids*; Seddon, K. R; Zaworothko, M. Eds.; NATO ASI Series C: Mathematical and Physical Sciences, Vol. 539; Kluwer: Boston, MA, 1999; pp 1-28.

2 Davis, R. F.; Glass, J. T. *Adv. Solid-State Chem.*, Catlow, C. R. A. Ed.; **1991**, *2*, 1-111.

3 a) Williams, J. R.; Johnson, M.; Johnson, D. C. *J. Am. Chem. Soc.*, **2001**, *123*, 1645-1649. b) Johnson, C. D., Noh, M., Sellinschegg, H., Schneidmiller, R., Johnson, D. C. In *Handbook Nanostructured Materials and Nanotechnology*, Nalwa, H. S. Ed.; Vol. 1, Academic Press: San Diego, **2000**, pp. 251-294. c) O'Hare, D., Evans, J. S. O., Francis, R., Price, S., O'Brien, S. *Mat. Sci. Forum*., **1998**, *278-281*, 367-378. d) Stein, A., Keller, S. W., Mallouk, T. E. *Science*, **1993**, *259*, 1558-1564.

4 Chen, C.-C.; Hergold, A. B.; Johnson, C. S.; Alivisatos, A. P. *Science*, **1997**, *276*, 398-401.

5 Hooke, Robert *Micrographia* Cramer, J., Swann, H. K., Eds.; Historiæ Naturalis Classica, Tomus XX; Wheldon & Wesley , Ltd. and Hafner: New York, 1664, reprint 1961; pp. 81-82.

6 Verma, A. R.; Krishna, P. *Polymorphism and Polytypism in Crystals*; Wiley and Sons: New York, 1966; pp. 61-91.

7 Jephcoat, A. P.; Mao, H.-K.; Finger, L. W.; Cox, D. E.; Hemley, R. J.; Zha, C.-S. *Phys. Rev. Lett.* **1987**, *59*, 2670-2673.

8 Izyumov, Y. A.; Syromyatnikov, V. N. *Phase Transitions and Crystal Symmetry*; Kluwer: Norwell, MA, 1984; pp.251-260.

9 Evans, R. C. *An Introduction to Crystal Chemistry*, Second Ed.; Cambridge University Press: Cambridge, U.K., 1966; pp. 62-63.

10 Rapoport, R.; Tistorius, C.W.F.T. *Phys. Rev.* **1968**, *172*, 838-847.

11 Bote, P. R.; Patil, P. K.; Nandgave, J. K.; Lawangar-Pawar, R. D. *Solid State Comm.* **1991**, *79*, 5-7.

12 Burley, G. *J. Phys. Chem.* **1964**, *68*, 1111-1114.

13 Winkler, H.; Brehler, B. *Naturwissenschaften* **1959**, 553-554.

14 Yakel, H.L.; Brynestead, J. *Inorg. Chem.* **1978**, *17*, 3294-3296.

15 O'Keefe, M. O.; Hyde, B. G. *Acta Cryst.* **1976**, *B32*, 2923-2936.

16 a) Ghoumari-Boûanani, H; Brun, G.; Liautard, B.; Tedenac, J. C. *Mat. Res. Bull.* **1993**, *28*, 901-908. b) Vouroutzis, N.; Manolikas, C. *Phys. Stat. Sol. A* **1989**, *111*, 491-497. c) Plyusnin, A. B.; Dubrovina, A. N. *Kristallografiya* **1979**, *24*, 600-601.

17 Sullivan, R. M.; Martin, J. D. *J. Am. Chem. Soc.*, **1999**, *121*, 10092-10097.

18 Martin, J. D.; Dattelbaum, A. M.; Sullivan, R. M.; Thornton, T. A.; Wang, J. ; Peachey M. T. *Chem. Mater.*, **1998**, *10*, 2699-2713.

19 a) Liu, H.; Ciraolo, M. F.; Grey, C. P.; Hanson, J.; Martin, J. D.; Sullivan, R. M. *In-situ Studies of Ethylene Sorption in CuAlCl4* BNL National Synchrotron Light Source Activity Report, Rothman, E. Z.; Hastings, J. B.; Department of Energy, Brookhaven National Laboratory, Upton, NY, 1997, B-72. b) Martin, J. D.; Sullivan, R. M.; Hanson, J.; Liu, H.; Ciraolo, M. F.; Grey, C. P. *Observation of Reactive Intermediates on Sorption of Ethylene into CuAlCl4* BNL National Synchrotron Light Source Activity Report, 1998, http://nslsweb.nsls.bnl.gov/nsls/pubs/actrpt/1998/MA1218.PDF (accessed Feb. 2001). c)

Sullivan, R. M.; Smith, D. S.; Martin, J. D; Hanson, J.; Liu, H.;, Grey, C. P. *The Effect of Low Pressures of Ethylene on β-CuAlCl4* BNL National Synchrotron Light Source Activity Report, 2000, http://nslsweb.nsls.bnl.gov/nsls/pubs/abstracts/2000/X7B/sull1366.pdf (accessed Feb. 2001).

20 Martin, J. D.; Leafblad, B. R.; Roger M. Sullivan, R. M.; Boyle, P. D. *Inorg. Chem.* **1998**, *37*, 1341-1346.

21 Norby, P. *J. Appl. Crystallogr.* **1997**, *30*, 21-30.

22 Amemiga, Y. *Synchrotron Radiation News* **1990**, *3*, 21.

23 a) Hammersley, A. P. *FIT2D: An Introduction and Overview;* ESRF Internal Report, ESRF97HA02T; European Synchrotron Radiation Facility: Grenoble Cedex, France, 1997. b) Hammersley, A. P. *FIT2D V9.129 Reference Manual V3.1*; ESRF Internal Report, ESRF98HA01T; European Synchrotron Radiation Facility: Grenoble Cedex, France, 1998.

24 Norby, P. In-situ Time Resolved Synchrotron Powder Diffraction Studies of Syntheses and Chemical Reactions. In *European Powder Diffraction*; Cernik, R. J., Delhez, R., Mittemeijer, E. J. Ed.s; Materials Science Forum Vol. 228 until 231: Trans Tech Publications; Zürich, Switzerland, 1996; pp. 147-152.

25 Larson, A. C.; Von Dreele, R. B. *GSAS General Structure Analysis System*; Report LAUR 86-748; Los Alamos National Laboratory: New Mexico, 1995.

26 Lutz, O. ; Oehler, H.; Kroneck, P. Z. Physik. A **1978**, 288, 17-21.

27 Ferguson, D. B., Haw, J. F. *Anal. Chem.* **1995**, *67*, 3342-3348.

28 Haw, J. F.; Richardson, R. R.; Oshiro, I.; Lazo, N. D.; Speed, J. A. *J. Am. Chem. Soc.* **1989**, *111*, 2052-2058.

29 Smith, S. A.; Levante, T. O.; Meier, B. H., Ernst, R. R. *J. Magn. Reson. A* **1994**, 106, 75.

30 Lim, K. H., Ph. D. Thesis, SUNY at Stony Brook, 1999.

31 a) Schurko, R. W.; Wasylishen, R. E.; Phillips, A. D. *J. Magn. Reson.* **1998**, *133*, 388-394. b) Han, O. H.; Oldfield, E. *Inorg. Chem.* **1990**, *29*, 3666-3669.

32 Samoson, A. *Chem. Phys. Lett.* **1985**, *119*, 29-32.

33 Yamada, K; Tomita, Y.; Okuda, T. *J. Mol. Struct.* **1995**, *345*, 219-227.

34 Grant, D. M. Chemical Shift Tensors. In *Encyclopedia of Nuclear Magnetic Resonance*; Grant, D. M., Harris, R. K., Ed.s; John Wiley: Chichester, U.K., 1996; pp 1298-1308.

35 Sullivan, R.; Liu, H., Smith, D. S., Hanson, J. C.; Osterhoudt, D.; Cerilo, M. Grey, C. P.; Martin, J. D., Manuscript in Preparation.

36 Vega, A. J. Quadrupolar Nuclei in Solids. In *Encyclopedia of Nuclear Magnetic Resonance*; Grant, D. M., Harris, R. K., Ed.s; John Wiley: Chichester, U.K., 1996; pp 3869-3888.

37 β-CuAlCl4: site symmetry 1, Cu-Cl; 2.359 Å, 2.369 Å, 2.356 Å, 2.361 Å, Cl-Cu-Cl; 111.3º, 109.0º, 110.9º, 110.5º, 109.1º, 106.4º. α-CuAlCl4: site symmetry $\bar{4}$, Cu-Cl; 2.359 Å, Cl-Cu-Cl; 107.9º, 112.7º. CuCl: site symmetry $\bar{4}3m$, Cu-Cl; 2.3772 Å, Cl-Cu-Cl; 109.47º.

38 a) Johnson, G. M.; Mead, P. J.; Dann, S. E.; Weller, M. T. *J. Phys. Chem. B.* **2000**, *104*, 1454-1463. b) Newsam, J.M., *J. Phys. Chem.* **1987**, *91*, 1259-1262. c) Ramdas, S.; Klinowski, J., *Nature* **1984**, *308*, 521-523.

39 Unpublished 63Cu MAS NMR spectrum of α-CuGaCl4 .

40 Koller, H.; Meijer, E. L.; Santen, R. A. v. *Solid State Nucl. Mag. Reson.* **1997**, *9*, 165.

41 Evans, J. S. O.; Wong, H.-V.; Price, S. J.; O'Hare, D. *J. Am. Chem. Soc.* **1998**, *120*, 10837-10846.

42 Brown, W. E.; Dollimore, D.; Galwey, A. K. *Reactions in the Solid State;* Bamford, C. H.; Tipper, C. F. H., Eds.; Comprehensive Chemical Kinetics Series, Vol. 22; Elsevier, New York, 1980; pp. 42-115.

43 a) Avrami, M. *J. Chem. Phys.* **1939**, *7*, 1103-1112. b) Avrami, M. *J. Chem. Phys.* **1940**, *8*, 212-224. c) Avrami, M. *J. Chem. Phys.* **1941**, *9*, 177-184.

44 Erofe'ev, B. V. C. R. *Dokl. Akad. Nauk. SSSR* **1946**, *52*, 511-514.

45 Sharp, J. H.; Hancock, J. D. *J. Amer. Cerm. Soc.* **1972**, 55(2), 74-77.

46 Arrhenius, S. *Z. Phys. Chem. Abt. A* **1889**, *4*, 226-248.

47 Cardew, P. T.; Davey, R. J.; Ruddick, A. J. *J. Chem. Soc., Faraday Trans. 2,* **1984**, 80, 659-668.

48 Franzen, H. F. *Physical Chemistry of Inorganic Crystalline Solids*; Springer-Verlag, New York , 1986, 88-105.

49 Toledano, P.; Dmitriev, V. *Reconstructive Phase Transitions in Crystals and Quasicrystals*; World Scientific: New York, 1996; pp. 265-287.

50 Polanyi, M.; Wigner, E. *Z. Phys. Chem. Abt. A* **1928**, 139, 439-452.

51 Hildebrand, D.L. *J. Chem. Phys.* **1970**, 52, 5751-5759.

52 Guido, M.; Gigli, G.; Balducci, G. *J. Chem. Phys.* **1972**, 57, 3731-3735.

53 Schmidt, A; Kababya, S.; Appel, M.; Khatib, S.; Botoshansky, M.; Eichen, Y. *J. Amer. Chem. Soc.* **1999**, 121, 11291-11299.

54 Yamada, K.; Kinoshita, M.; Hosokawa, K. *Bull. Chem. Soc. Jpn.* **1993**, *66*, 1317-1322.

55 a) Nakamoto, K. *Infrared and Raman Spectra of Inorganic and Coordination Compounds: Part A. Theory and Applications in Inorganic Chemistry*, Fifth Ed.; John Wiley: New York, 1997; pp. 124-136. b) Fateley, W. G.; Dollish, F. R.; McDevitt, N. T.; Bentley, F. F. *Infrared and Raman Selection Rules for Molecular and Lattice vibrations: The Correlation Method*; Wiley-Interscience: New York, 1972; p. 26.

56 Woodward, R. B.; Hoffmann, R. "*The Conservation of Orbital Symmetry*"; Verlag Chemie: Weinheim/Bergstr., Germany and Academic Press: New York, **1970**.

57 Manson, J. E. *J. Phys. Chem.* **1956**, *60*, 806-807.